Integral SPH: Connecting the partition of unit to accurate gradient estimation

Domingo García-Senz
Departament de Fìsica,
Universitat Politècnica de Catalunya (UPC) and
Institut d'Estudis Espacials de Catalunya (IEEC)
Barcelona, Spain
domingo.garcia@upc.edu

Rubén M. Cabezón
sciCORE,
Universität Basel
Basel, Switzerland
ruben.cabezon@unibas.ch

***Abstract*—The correct evaluation of gradients is at the cornerstone of the smoothed particle hydrodynamics (SPH) technique. A novel scheme to estimate gradients using an integral approach has been recently proposed. Such approach retains the Lagrangian structure of SPH equations and is fully conservative. In this paper we study the connection between the choice of the volume elements, which enter in the SPH summations, and the accuracy in the gradient estimation within the integral approach scheme. Using analytic considerations, simple static toy models in 1D and a few dynamical 2D and 3D test cases, it is shown that any improvement in the partition of unit, not only leads to a reduction of the E0-errors, but also to a better calculation of gradients when the integral approach is used jointly.**

I. Introduction

Currently, the smoothed particle hydrodynamics (SPH) is a firmly settled technique, able to successfully cope with many cutting-edge problems in physics, astrophysics and engineering. This technique has undergone a sustained enhancement since its formulation [1], [2] and it is still evolving at a good pace [3], [4]. One landmark in that evolution concerns the estimation of derivatives and gradients, which can be done by many different approaches. The standard way of calculating gradients by directly taking the analytic derivative of the interpolating kernel function leads to E0-errors, even in presence of constant pressure fields in non uniform particle distributions [5]. Another proposal adapts the moving-least squares technique (MLS) to SPH [6] to ensure an exact interpolation of linear functions. Adding renormalization corrections to both the kernel and the kernel gradient has proved to enhance the accuracy in the calculation of gradients and to reduce the tensile instability [7]. A variational principle plus kernel renormalization was used by [8] to simulate fluid systems with free surfaces. Nevertheless, these MLS and renormalization techniques, in general, do not guarantee the perfect conservation of the whole set of physical laws governing the fluid motion, which are at the foundational roots of the SPH technique. A recent proposal was the Conservative Reproducing Kernel SPH method, CRKSPH, [9] which enforces perfect linear interpolation and, at the same time, retain the linear momentum and energy conservation properties (but it does not perfectly conserve angular momentum).

Another way to estimating gradients was recently devised by [10]. In their proposal, gradients are calculated from an integral expression, so that there is not need to explicitly calculate the analytic derivative of the kernel function. They also proved that such integral can be made totally compatible with the Lagrangian formulation of the SPH equations, leading to the Integral Smoothed Particle Hydrodynamics (ISPH) scheme (named IAD_0 in [10]). It was shown that the ISPH formulation has the same conservation properties as the standard, Lagrangian-born, SPH [11]. In particular, a remarkable feature of ISPH is that it reduces the E0-error in the derivatives [10], [12]. In this work we dig further into the conditions that the ISPH scheme should met in order to improve the calculation of gradients, which can become exact for linear functions. It turns out that these conditions are connected with another basic SPH requirement: the correct partition of the unit volume. Using one-dimensional numerical experiments we make clear the link between these two basic properties: any enhancement in the partition of unit leads to a better gradient estimation. The results of these 1D simple models are confirmed by detailed 2D and 3D hydrodynamic simulations of explosions and instabilities.

In Section II we review the main features of the ISPH scheme and the implementation of the generalized volume elements (VE) used to compute the summations. The link between the performance of the ISPH calculation of gradients and the adequate choice of the VE is highlighted in Section III. In Section IV we apply our code to a couple of standard tests calculated in two and three dimensions, and analyze the results in the light of the VE choice. A summary of our findings and the prospects for future work are given in the conclusions section.

II. The ISPH formulation

A. Gradient calculation with ISPH

The classical way to evaluating gradients in SPH takes the multidimensional derivative of a function f as

$$\nabla f = \int_V f(\mathbf{r}')\ \nabla \mathbf{W}(\mathbf{r},\mathbf{r}')\ dr'^3\,, \tag{1}$$

where $W(\mathbf{r},\mathbf{r}')$ is commonly a Dirac δ-like function named *interpolating kernel*, which is continuous and derivable. In the classical SPH formulation the gradient of the function is estimated: approaching the integral (1) by summations, taking the analytic derivative of the kernel, and assuming that the volume element dr'^3 is adequately represented by m_b/ρ_b. Namely,

$$\langle \nabla f \rangle_a = \sum_b \frac{m_b}{\rho_b} f_b \nabla \mathbf{W}(\mathbf{r_a},\mathbf{r_b})\,. \tag{2}$$

Alternatively, in ISPH the gradient is calculated from an integral approach (IA), which does not require the explicit analytic derivative of $W(\mathbf{r},\mathbf{r}')$. The following integral is defined by [10],

$$I(\mathbf{r}) \equiv \int_V \left[f(\mathbf{r}') - f(\mathbf{r})\right](\mathbf{r}'-\mathbf{r}) W(|\mathbf{r}'-\mathbf{r}|,h) dr'^3\,, \tag{3}$$

where $W(|\mathbf{r}'-\mathbf{r}|,h)$ is a spherically symmetric normalizable interpolating function and h is the smoothing length. The integral $I(\mathbf{r})$ can be used to find the gradient of a function $f(\mathbf{r})$ in a similar way that the Laplace operator is usually approached from another integral expression in standard SPH, [13], [14]. The *IA* interpretation of SPH is the consequence of approaching (3) with summations along with,

$$f(\mathbf{r_b}) - f(\mathbf{r_a}) = \nabla \mathbf{f_a} \cdot (\mathbf{r_b}-\mathbf{r_a})\,, \tag{4}$$

where a and b refer to neighbouring particles with masses m_a and m_b, respectively. The RHS in the integral expression (3) writes,

$$I(\mathbf{r_a}) = \left[\sum_b \frac{m_b}{\rho_b} f(\mathbf{r_b})(\mathbf{r_b}-\mathbf{r_a}) W(|\mathbf{r_b}-\mathbf{r_a}|,h_a)\right] - \left[f(\mathbf{r_a})\langle \mathbf{\Delta r}\rangle_a\right], \tag{5}$$

where,

$$\langle \mathbf{\Delta r}\rangle_a = \sum_b \frac{m_b}{\rho_b}(\mathbf{r_b}-\mathbf{r_a}) W(|\mathbf{r_b}-\mathbf{r_a}|,h_a)\,. \tag{6}$$

Putting (4) and (5) into (3) allows to obtain the gradient $\nabla \mathbf{f_a}$,

$$\begin{bmatrix} \partial f/\partial x_1 \\ \partial f/\partial x_2 \\ \partial f/\partial x_3 \end{bmatrix}_a = \begin{bmatrix} \tau_{11} & \tau_{12} & \tau_{13} \\ \tau_{21} & \tau_{22} & \tau_{23} \\ \tau_{31} & \tau_{32} & \tau_{33} \end{bmatrix}^{-1} \begin{bmatrix} I_1 \\ I_2 \\ I_3 \end{bmatrix}, \tag{7}$$

where

$$\tau_{ij,a} = \sum_b \frac{m_b}{\rho_b}(x_{i,b}-x_{i,a})(x_{j,b}-x_{j,a}) W_{ab}(h_a)\,; i,j = 1,3\,. \tag{8}$$

It was shown in García-Senz et al. [10] that (7) leads to both, exact conservation of the SPH Euler equations and perfect linear interpolation *only* when $\langle \mathbf{\Delta r}\rangle \to 0$. We will refer as ISPH to the conservative scheme which simply *neglects*[1] the term $f(\mathbf{r_a})\langle \mathbf{\Delta r}\rangle_a$ in (5). Hence, an exact linear interpolation is not always guaranteed by the ISPH scheme. A fully description of the ISPH equations can be found in [12], [15]. On another note, the complete integral approach, which takes into account the $f(\mathbf{r_a})\langle \mathbf{\Delta r}\rangle$ term in the RHS of (5), leads to perfect linear interpolation but is not fully conservative. We refer to it as non conservative ISPH (ncISPH, hereafter). As commented above, both schemes, ISPH and ncISPH, converge to the same outcome when $\langle \mathbf{\Delta r}\rangle \simeq 0$.

B. Choice of the volume elements

In SPH volume integrals are usually approached by finite summations by $V_a = m_a/\rho_a$, where m_a is the mass of the particle. For example, an estimate of the density writes,

$$\rho_a = \sum_{b=1}^{n_b} V_b \rho_b W_{ab}(|\mathbf{r_b}-\mathbf{r_a}|,h_a) = \sum_{b=1}^{n_b} m_b W_{ab}(|\mathbf{r_b}-\mathbf{r_a}|,h_a)\,, \tag{9}$$

Nevertheless, other options for V_a may be of interest to address specific problems. The code SPHYNX [15], makes use of the concept of generalized volume elements developed by [16], [17]. First a scalar estimator X_a is defined so that the particle volume is,

$$V_a = \frac{X_a}{\sum_b X_b W_{ab}}\,. \tag{10}$$

The density of the particle is then calculated as $\rho_a = m_a/V_a$. Current choices for the estimator that can be found in the literature are $X_a = 1, m_a, P_a^k$, where P is the pressure and $k \leq 1$. There is however a particular choice which, according to [15], provides a better partition of the unit. Namely,

$$X_a = \left(\frac{m_a}{\rho_a}\right)^p\,. \tag{11}$$

Setting $p = 0$ produces the standard volume element for particles with identical mass, whereas $0 < p \leq 1$ gradually improves the kernel normalization.

In the following sections we show that reducing the error in the kernel normalization (E_1, hereafter) of particle a,

$$E_1 = [\sum_b V_b W_{ab} - 1]\,, \tag{12}$$

usually improves the requirement:

$$E_2 \cdot h_a = |\langle \mathbf{\Delta r}\rangle|_a = \left|\sum_b V_b\ (\mathbf{r_b}-\mathbf{r_a})\ W(|\mathbf{r_b}-\mathbf{r_a}|,h_a)\right| \simeq 0\,, \tag{13}$$

where E_2 is the normalized error module $|\langle \mathbf{\Delta r}\rangle|_a/h_a$ of particle a. Any reduction in both errors will improve the dynamic evolution of the physical system.

[1] This is justified because $\langle \mathbf{\Delta r}\rangle$ is in fact the integral of an odd function, which is zero. Interestingly, this argument has been used during the whole history of SPH to justify that it is a second order method, which is in general true, but not ensured unless a scheme like the one presented here is used.

III. Estimating the errors E_1, E_2 for different particle distributions

A good control of errors E_1 and E_2 is of upmost importance to the SPH technique. This is so because the quality of both, the interpolated function $\langle f \rangle (\mathbf{r})$,

$$\langle f \rangle (\mathbf{r}) \simeq f(\mathbf{r}) \sum_b V_b W_{ab} + \nabla \mathbf{f} \cdot \sum_b V_b (\mathbf{r_b} - \mathbf{r_a}) W_{ab} \,, \quad (14)$$

and its gradient $\langle \nabla f \rangle (\mathbf{r})$ (7), are very sensitive to these errors [12]. Nevertheless, both errors are correlated, as it can be inferred from the following qualitative argumentation in one dimension. We first take the kernel normalization condition as a function of the spatial coordinate,

$$G(x_a) = \sum_b V_b W_{ab}(|x_a - x_b|, h_a) \,. \quad (15)$$

Using the gaussian kernel $W_{ab} = \frac{C}{h_a} \exp[-(\frac{x_a - x_b}{h_a})^2]$, the standard SPH derivative of $G(x)$ writes,

$$\left(\frac{dG}{dx} \right)_a = -\frac{2}{h_a^2} \sum_b V_b (x_a - x_b) W_{ab} \,, \quad (16)$$

thus,

$$\sum_b V_b (x_a - x_b) W_{ab} = -\frac{h_a^2}{2} \left(\frac{dG}{dx} \right)_a \,. \quad (17)$$

We note that the LHS of (17) is in fact E_2, suggesting that having a good partition of unit ($G \simeq 1$, everywhere) makes $dG/dx \simeq 0$ and, as consequence the E_2 error is suppressed. An independent proof of the link between E_1 and E_2 obtained with an exponential kernel [18], was given in the Appendix A by [15].

It should be recognized, however, that the proof above is only indicative because, unlike the interpolators widely used in practical calculations, the gaussian and the exponential kernels are functions without compact support. Moreover, it could happen that even when $G(x)$ is close to one, it shows fluctuations around the particle and its derivative may significantly differ from zero.

In this regard, additional insight about the impact of the VE choice in the errors E_1, and E_2 can be obtained by studying a handful of static particle distributions and using compact-supported kernels. These errors are expected to be large close to discontinuities, which in SPH are usually spread over a few times the smoothing-length distance (h). We have chosen three representative discontinuities which often appear in practical calculations: a Gaussian (model A), an Inverted-Gaussian (model B) and a Wall (model C). These are given by the following mathematical expressions:

$$\rho(x) = \rho_0 + \Delta\rho \; e^{-(\frac{x - x_0}{\delta})^2}, \qquad (A) \quad (18)$$

$$\rho(x) = \rho_0 - \Delta\rho \; e^{-(\frac{x - x_0}{\delta})^2}, \qquad (B) \quad (19)$$

TABLE I
Value of the different magnitudes in profiles A, B and C

Profile	ρ_0	$\Delta\rho$	δ	h
A	1.0	1.0	0.040	0.0230
B	2.0	1.0	0.008	0.0051
C	1.5	0.5	0.020	0.0230

$$\rho(x) = \rho_0 + \Delta\rho \; \frac{e^{(\frac{x - x_0}{\delta})} - e^{-(\frac{x - x_0}{\delta})}}{e^{(\frac{x - x_0}{\delta})} + e^{-(\frac{x - x_0}{\delta})}}, \qquad (C) \quad (20)$$

where the values of the parameters $\rho_0, \Delta\rho, \delta$ are specified in Table I.

We arranged these profiles into a 1D distribution of particles with reflective boundary conditions. The smoothing-length h was set constant along the grid so that the grad-h contribution is negligible and we used an interpolating $sinc$-kernel with exponent $n = 5$ [19], which has a shape similar to the M_6 spline. The different profiles of errors E_1, E_2 at each point are depicted in Fig. 1. As we can see, there is an evident improvement in the kernel normalization condition as p in (11) increases. For $p \simeq 1$ the E_1 error becomes negligible. The normalized error $E_2 = |\langle \mathbf{\Delta x} \rangle| / h$ follows a similar trend, suggesting that having a good partition of unit is not only beneficial to approach the density, but also to calculating the derivatives of any magnitude of interest.

The link between E_1, E_2, and the volume elements still holds in presence of some amount of numerical noise. To probe this, we perturbed the lattice of particles in model A (Gaussian profile) so that the particles are randomly displaced up to a 5% around its unperturbed position. Although, according to Fig. 2 the errors E_1 and E_2 become slightly larger compared with the non-perturbed test, the increase of the exponent p in (11) is again improving both, the partition of unit and the $\langle \mathbf{\Delta x} \rangle$ condition.

A. Impact of VE in estimating gradients

We can use our simple sharp profiles above to gain insight into the relationship between E_1, E_2, and the accuracy of the first derivative. To do that, we assume that the density of the test particle distribution follows profile A (18), so that it totally determines the VE through (11). Let us also assume that we wish to obtain the SPH derivative of the wall-like function f given by profile C, (20). Such derivative, $\frac{df}{dx}$, is sensitive to the choice of the exponent p in (11). We can thus compare the analytic and the numerical value of $\frac{df}{dx}$ and carry out the L_1 analysis of the results.

A summary of the numerical experiments is shown in Fig. 3. The first panel shows the density profiles: analytic (red) and the estimations with $p = 0.0$ (green) and $p = 0.8$ (blue) in the VE. The analytic function f is depicted in yellow. The second panel shows the gradient of f. For comparison, the black line shows the derivative of f calculated in the usual SPH way [14],

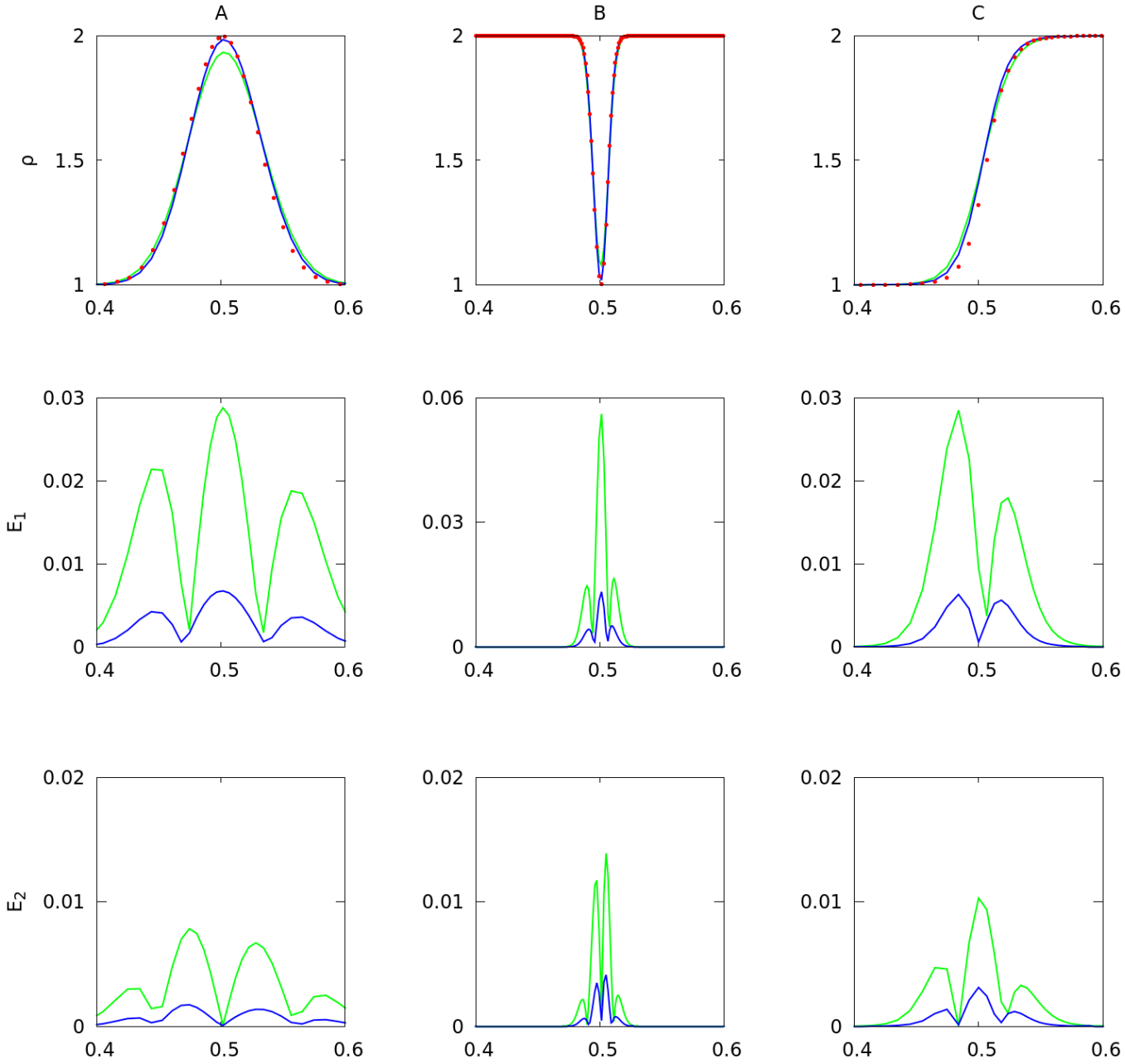

Fig. 1. Results of the SPH evaluation of the test profiles A, B, and C using different VE. Upper row: density profiles of models A (Gaussian), B (Inverted-Gaussian), and C (Wall), in Table I, calculated using $p = 0.0$ (green) and $p = 0.8$ (blue) in (11). Points in red are the analytic values. Central row: E_1 (partition of unit) error for the same three profiles. Bottom row: Same as central row but for error $E_2 = |\langle \mathbf{\Delta x} \rangle|/h$.

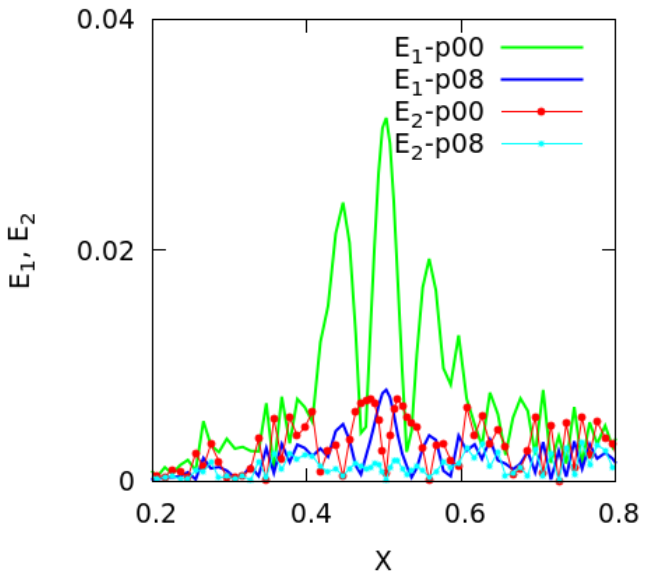

Fig. 2. Errors E_1 and E_2 for the same Gaussian density profile shown in Fig. 1 (left column), but with the particles randomly displaced from their lattice position.

$$\left(\frac{df}{dx}\right)_a = \frac{1}{\rho_a}\sum_b m_b(f_b - f_a)\frac{dW_{ab}}{dx}\,. \qquad (21)$$

The density profile is in general well reproduced, but only the case $p = 0.8$ gets close to the analytic value at the maximum at $x = 0.5$ and has the correct description of the tails of the distribution, giving a better description of the system even in low resolution regions. Although the value around the maximum of $\frac{df}{dx}$ is similar for $p = 0.0$ and $p = 0.8$, the last option fits much better the derivative around the coordinate $x = 0.6$. As we can see, using $p = 0.0$ and (21) (black line), which is equivalent to the standard SPH version, gives the poorest result. This assessment is confirmed below by the L_1 analysis of the profiles in Fig. 4. The third and fourth panels in Fig.3 depict the profiles of kernel normalization (left) and $|\langle \mathbf{\Delta x}\rangle|/h$ (right) for different values of exponent p. Again, higher p values lead to a better estimation of both magnitudes.

Figure 4 shows the convergence rate between the ISPH and ncISPH schemes in light of the L_1 error of the derivative,

$$L_1 = \frac{1}{N}\sum_{b=1,N}\left|\left(\left(\frac{df}{dx}\right)_{analytic} - \left(\frac{df}{dx}\right)_{sph}\right)_b\right| \qquad (22)$$

First of all, we note that because the ncISPH scheme is making exact linear interpolations, the results (green line) are not sensitive on the adopted p value. On the contrary, the results of the conservative scheme, ISPH, do show a clear dependence on the choice of the volume elements, as expected. The $L_1(p)$ profile is almost linearly decreasing for $p \leq 0.6$, it saturates asymptotically when $p \geq 0.8$ at the same accuracy as the ncISPH scheme, but conserving momentum. This result also indicates that, in general, the use of higher p values (i.e. $p \gtrsim 0.6$) is recommended.

Even though the test cases presented in this section were calculated in 1D with ordered and pseudo-ordered particle settings, the results unambiguously support the idea that *a better partition of unit improves the calculation of gradients in SPH*.

IV. Multi-dimensional simulations

In this section we analyze the results of two well-known dynamical tests, that require the solution of the full system of Euler equations. In particular, we studied the evolution of a point-like explosion (the Sedov test), as well as the growth of the Kelvin Helmholtz (KH) instability. The simulations were carried out using the ISPH code SPHYNX and the outcomes have been compared to well-known solutions as well as to the results obtained with the same code but using the classical scheme for calculating gradients (referred as stdSPH below).

A. The Sedov explosion

We simulated this popular test in a three-dimensional square box of side $L = 1$. The explosion was initiated at the center of the box by depositing an amount of energy $\Delta U = 1$. That energy was spread following a Gaussian profile with characteristic width $\delta = 0.1$ (see [15] for more details).

To investigate the dependence of the errors E_1, (12) and (13) with respect the parameter p in (11), we calculated the following L_1 values in the shocked volume at each integration step,

$$L_1(E_{1,2}) = \langle |E_{1,2}| \rangle\ , \qquad (23)$$

where the brackets stand for the arithmetic average of the errors. For this test, we used two different VE, $p = 0.0$ and $p = 0.7$, as well as the stdSPH. The outcome of the simulations is summarized in Fig. 5, which shows the profiles of density, and pressure at time $t = 0.05$, as well as the temporal evolution of $L_1(E_1)$ and $L_1(E_2)$. The best match with the analytic profile (red) was obtained with ISPH and $p = 0.7$ (blue) not only in the peak values, but also in the low density region close to the center of the explosion, where the pressure is well reproduced only by this combination. The choice $p = 0.0$ (green) leads to similar results to those obtained with stdSPH (black).

The temporal evolution of the error estimators $L_1(E_1, E_2)$ (bottom panel) confirms that combining ISPH with a high value of the exponent p reduces both errors and improve the simulations.

B. The Kelvin-Helmholtz instability

The simulation of the development of the Kelvin-Helmholtz instability is a suitable test to measure the impact of changing the volume elements in problems involving shear instabilities.

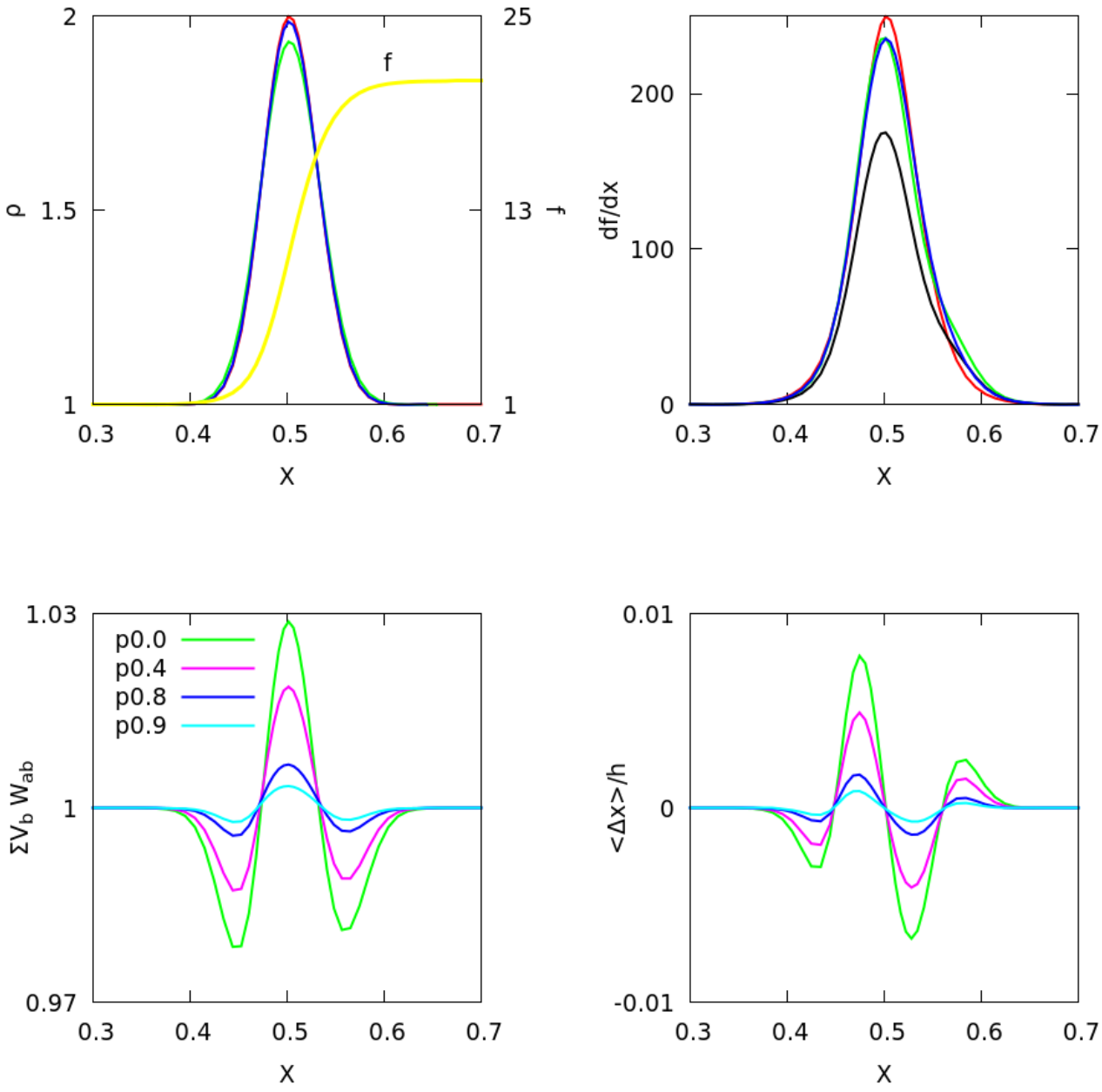

Fig. 3. Upper-left: Profiles of a Gaussian-like density function (red) and a wall-like function ($f(x)$, in yellow). Upper-right: Gradient of function $f(x)$ estimated with different VEs. The black line is the standard SPH derivative. Bottom-left: Convergence in kernel normalization. Bottom-right: Convergence to zero of $\langle \Delta x \rangle / h$.

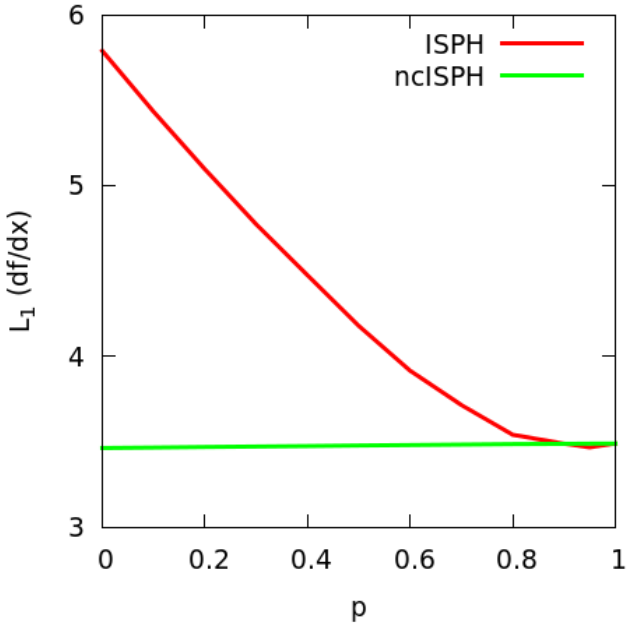

Fig. 4. Convergence between ISPH (conservative but not always providing exact linear interpolations) and ncISPH (exact linear interpolations but non-conservative) schemes as a function of the exponent p in (11).

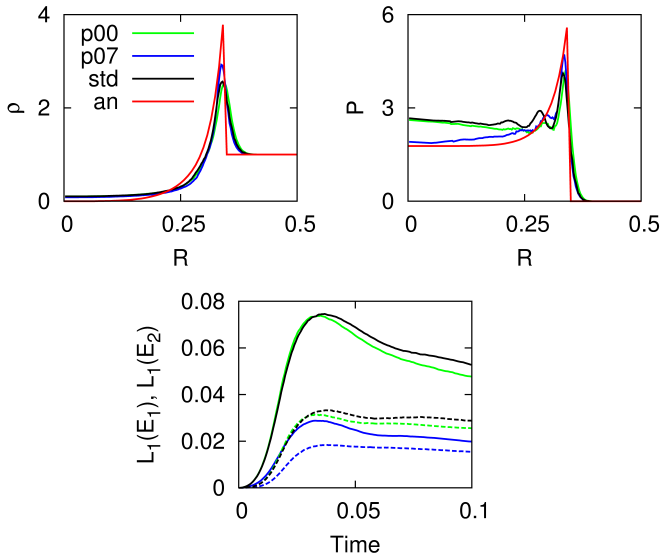

Fig. 5. Sedov explosion. Upper-left panel: density profiles calculated with different VEs. The analytic solution is given by the red line. Upper-right panel: same for pressure. Bottom: Evolution of L_1, related to the errors E_1 and E_2, (23)

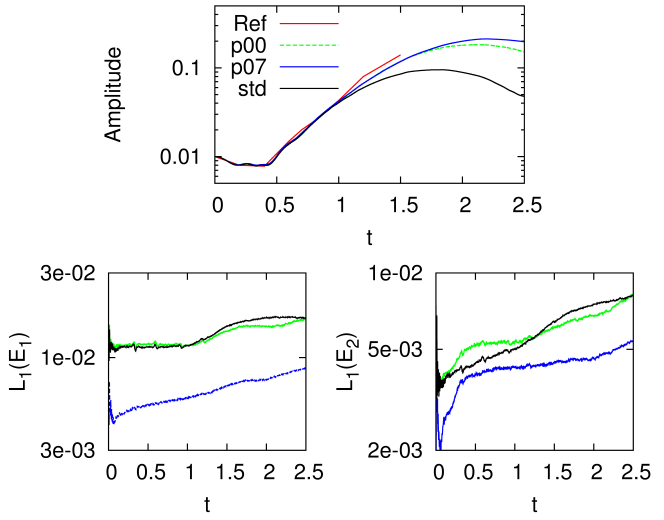

Fig. 6. The Kelvin-Helmholtz instability. Upper panel: Perturbation amplitude calculated with different VEs. The reference profile by McNally ([20]) is given by the red line. Bottom-left panel: evolution of the L_1 value related to the error E_1, Eq. (23). Bottom-right Evolution of the L_1 value related to the error E_2.

Fortunately, there is a reference solution, obtained by McNally [20], to compare with. As in the Sedov test, we refer the reader to the reference [15] to get the details of the setup of this experiment.

We run this test in two-dimensions using our ISPH code with $p = 0.0$ and $p = 0.7$, as well as with stdSPH. During the evolution of the instability, we calculated the error estimators $L_1(E_1)$ and $L_2(E_2)$, (23). Figure 6 shows the results of the simulations. The upper panel depicts the evolution of the perturbation amplitude for the two ISPH calculations with $p = 0.0$ (green) and $p = 0.7$ (blue). These profiles are compared with the reference solution (red) and with the stdSPH calculation (black). All cases evolve in a similar manner during the linear stage of growth, until $t \simeq 1$. Nevertheless, once the perturbation enters in the non linear regime, the profiles diverge. At this point, the ISPH scheme is matching the reference calculation much better than stdSPH. The evolution of ISPH cases with $p = 0.0$ and $p = 0.7$ is very similar until $t \simeq 2$. From this moment on, the $p = 0.7$ case shows a larger amplitude development. It is worth noting that both particle schemes, stdSPH and ISPH share exactly the same physics and artificial viscosity recipe. Thus, the differences in the outcome are mainly due to the different approaches used in the estimation of gradients.

The L_1 and L_2 errors are shown in the bottom panel of Fig. 6. Again the VE option with $p = 0.7$ led to both, a better partition of unit and smaller $|\langle \mathbf{\Delta r} \rangle|/h$.

V. Conclusion

The main contribution of this communication is to highlight the connection between the partition of unit and gradient estimation accuracy in SPH. In particular, we show that improving the constraint $\sum_b V_b W_{ab}(h_a) = 1$ automatically leads to an

enhancement of the condition $\sum_b V_b(\mathbf{r_b} - \mathbf{r_a})W_{ab}(h_a) = 0$. In the ISPH paradigm, the fulfillment of the last expression is a sufficient condition to perform exact linear interpolations. Thus, provided that the volume elements V_a are correctly chosen, the ISPH scheme makes compatible complete conservation of mass, momentum, energy and entropy with an exact estimation of the gradient of linear functions. Nevertheless, having a good partition of unit will be beneficial to any SPH scheme.

We also present a family of suitable volume elements obtained through the concept of generalized VE proposed by Hopkins [16]. These volume elements are included in the summations in a *explicit* way and updated at each integration step. Such simple recipe provides good results. In our experience, the only drawback is that some overshooting of the density can occur in presence of large density discontinuities when $p > 0.7$ is used. According to [15] that shortcoming can be alleviated by either slightly reducing the value of the exponent p in (11) or by changing that expression to $X_a = (\langle m_a/\rho_a \rangle)^p$, with $p \simeq 1$ (where $\langle . \rangle$ means the SPH average).

A best procedure would probably be to *implicitly* obtain the volume elements V_a directly from the constraint $\sum_b V_b W_{ab} = 1$. While the implicit quest of V_a is feasible en 1D, it may be computationally too costly in current multidimensional simulations.

Even though we establish a clear link between the errors E_1 and E_2, and the ISPH method of estimating gradients, our results are obtained with ordered and pseudo-ordered initial models, for the most part. It is our plan to investigate to what extent our conclusions are still valid in presence of greater particle disorder in a future work.

ACKNOWLEDGMENT

This work has been supported by the MINECO Spanish project AYA2017-86274-P and the Generalitat of Catalonia SGR-661/2017 (D.G.), by the Swiss Platform for Advanced Scientific Computing (PASC) project SPH-EXA: Optimizing Smooth Particle Hydrodynamics for Exascale Computing (R.C. and D.G.). The authors acknowledge the support of sciCORE (http://scicore.unibas.ch/) scientific computing core facility at University of Basel, where part of these calculations were performed.

REFERENCES

[1] Lucy, L. B., "A numerical approach to the testing of the fission hypothesis", AJ, 82, 1013, 1977

[2] Gingold, R. A., Monaghan, J. J., "Smoothed particle hydrodynamics - Theory and application to non-spherical stars", MNRAS, 181, 375, 1977

[3] Liu, M.B., Liu, G.R., "Smoothed Particle Hydrodynamics (SPH): an Overview and recent Developments", Arch. Comput. Methods Eng., Vol 17, p25, 2010

[4] Monaghan, J. J., "Smoothed Particle Hydrodynamics and Its Diverse Applications", Annual Review of Fluid Mechanics, 44, 323, 2012

[5] Agertz, O., Moore, B., Stadel, J., Potter, D., Miniati, F., Read, J., Mayer, L., Gawryszczak, A., Kravtsov, A., Nordlund, Ł A., Pearce, F., Quilis, V., Rudd, D., Springel, V., Stone, J., Tasker, E., Teyssier, R., Wadsley, J., and Walder, R., "Fundamental differences between SPH and grid methods". MNRAS, 380, 963978, 2007

[6] Dilst, G., "Moving-least-squares-particle hydrodynamics-I. Consistency and stability", in Numerical Methods in Engineering, Vol 48, issue 8, 1115, 1999

[7] Bonet, J., Lok, T.-S.L., "Variational and momentum preservation aspects of Smoothed Particle Hydrodynamics formulations", Comput. Meth. Appl. Mech. Engrg., 180, 97, 1999

[8] Oger, G., Doring, M., Alessandrini, B., and Ferrant, P."An improved SPH method: Towards higher order convergence", J. Comput. Phys., 225, 1472, 2007

[9] Frontiere, N., Raskin, C. D. and Owen, J. M., "CRKSPH - A Conservative Reproducing Kernel Smoothed Particle Hydrodynamics Scheme", J. Comput. Phys., 332, 160, 2017

[10] García-Senz, D., Cabezón, R. M. and Escartín, J. A., "Improving smoothed particle hydrodynamics with an integral approach to calculating gradients", A&A, 538, A9, 2012

[11] Springel, V., Hernquist, L., "Cosmological smoothed particle hydrodynamics simulations: the entropy equation", MNRAS, 333, 649, 2002

[12] Rosswog, S., "Boosting the accuracy of SPH techniques: Newtonian and special-relativistic tests", MNRAS, 448, 3628, 2015

[13] Brookshaw, L.,"A method of calculating radiative heat diffusion in particle simulations", Proceedings of the Astronomical Society of Australia, 6, 207, 1985

[14] Monaghan, J. J., "Smoothed particle hydrodynamics", Reports on Progress in Physics, 68, 1703, 2005

[15] Cabezón, R. M., García-Senz, D. and Figueira, J., "SPHYNX: an accurate density-based SPH method for astrophysical applications", A&A, 606, A78, 2017

[16] Hopkins, P. F., "A general class of Lagrangian smoothed particle hydrodynamics methods and implications for fluid mixing problems", MNRAS, 428, 2840, 2013

[17] Saitoh, T. R., Makino, J., "A Density-independent Formulation of Smoothed Particle Hydrodynamics", ApJ, 768, 44, 2013

[18] Fulk, D. A., Quinn, D. W.,"An Analysis of 1-D Smoothed Particle Hydrodynamics Kernels", J. Comput. Phys., 126, 165, 1996

[19] Cabezón, R. M., García-Senz, D. and Relaño, A., "A one-parameter family of interpolating kernels for smoothed particle hydrodynamics studies", J. Comput. Phys., 227, 8523, 2008

[20] McNally, C. P., Lyra, W. and Passy, J.-C., "A Well-posed Kelvin-Helmholtz Instability Test and Comparison", ApJS, 201, 18, 2012